

Visualisation and knowledge discovery from interpretable models

Preprint of IJCNN 2020 as prepared by the authors*

Sreejita Ghosh¹, Peter Tino², and Kerstin Bunte¹

¹*Bernoulli Institute, University of Groningen, The Netherlands*

²*School of Computer Science, University of Birmingham, The United Kingdom*

Abstract

Increasing number of sectors which affect human lives, are using Machine Learning (ML) tools. Hence the need for understanding their working mechanism and evaluating their fairness in decision-making, are becoming paramount, ushering in the era of Explainable AI (XAI). In this contribution we introduced a few intrinsically interpretable models which are also capable of dealing with missing values, in addition to extracting knowledge from the dataset and about the problem. These models are also capable of visualisation of the classifier and decision boundaries: they are the angle based variants of Learning Vector Quantization. We have demonstrated the algorithms on a synthetic dataset and a real-world one (heart disease dataset from the UCI repository). The newly developed classifiers helped in investigating the complexities of the UCI dataset as a multiclass problem. The performance of the developed classifiers were comparable to those reported in literature for this dataset, with additional value of interpretability, when the dataset was treated as a binary class problem.

Keywords— adaptive distances, learning vector quantization, non-linear visualization, interpretability

1 Introduction

In this era of increasing number of machine learning (ML) algorithms being deployed in various sectors, including finance, healthcare, criminology, justice, politics, manufacturing, and logistics, more and more human lives are impacted by them. Consequently there is a rising need of transparency and interpretability of the models [1–3] to achieve comprehensible decisions. ML algorithms with greater predictive powers are often more complex and behave like a *black box*, i.e. the working logic of these models is concealed from the human experts, thus obviating any way of verifying the reasoning and thus, the fairness of system [3]. However role of ML in high-stake prediction applications concerning human lives demand that its decisions be explainable by

humans [3].

However, there have been debates about the meaning of the term interpretability, and how to compare interpretability of different classifiers, especially when comparing models of distinct types. To tackle this problem Backhaus and Seiffert proposed 3 criteria [2, 4]: (1) the model’s ability to perform feature selection from the input pattern, (2) the model’s ability to provide typical data points representing a class, and (3) model parameters having information about the decision boundary directly encoded. Different strategies have been proposed: including model-agnostic pre- or post-processing methods such as univariate feature selection [3] and post hoc visualisation of decision boundaries [5, 6]. This contribution focuses on intrinsically interpretable techniques and hence model-specific examples. Using these criteria Support Vector Machines (SVM) models [2] are graded 1 out of 3 because they satisfy only criteria (3), to contain information about the decision boundary. In Decision trees (DTs) [7] rules are interpretable. A typically higher performance classifier, Random Forest (RF), is built by bagging several DTs on random subsets of the data. However ensembling compromises on interpretability. Naive Bayes (NB) assumes independence of features which leads to interpretability of individual features and their contribution for decision making. However it lacks the ability to account for feature interactions for the target outcome [3]. In this paper we aim to develop a *competitive* classifier in terms of performance, which is also easily interpretable, and can be visualised, satisfying criteria 1-3 [4].

Nearest Prototype Classification (NPC) is an intuitive learning scheme where a novel sample gets assigned the class label of its closest prototype. Thus techniques implementing it, such as Generalized LVQ (GLVQ) [8] for example, often allow interpretation of the prototypes as representative of class information allowing transparency with respect to (2). The Generalized Relevance LVQ (GRLVQ) [9] extension to it additionally provide feature relevance determination by introduction of an adaptive parameterized dissimilarity. This weighs the importance of features for the classification and makes this extension fulfill criteria (1) as well. Further adaptations allow for multi-variate and class-wise feature analysis [10, 11] and visualisation of decision boundaries [5]. However certain datasets, such as medical data, often contain missing values, heterogeneous measurements, and frequently exhibit imbalanced classes which often hinder the straightforward application of ML algorithms.

We addressed the aforementioned challenges by introducing an angular adaptive dissimilarity measure and an oversampling

*©20XX IEEE. Personal use of this material is permitted. Permission from IEEE must be obtained for all other uses, in any current or future media, including reprinting/republishing this material for advertising or promotional purposes, creating new collective works, for resale or redistribution to servers or lists, or reuse of any copyrighted component of this work in other works

strategy in [12]. In this contribution we present and demonstrate extensions to [12] which allow for knowledge discovery from non-linearly separable datasets exhibiting the mentioned hindrances. The proposed interpretable classifiers are demonstrated on a synthetic and a publicly available dataset. These classifiers are capable of class-wise and multi-variate feature analysis and visualisation of non-linear decision boundaries (see section 2), thus satisfying at least 2 of the 3 criteria of [4]. Detailed explanation of GLVQ and its extensions relevant to this paper can be found in section 2.

2 Methods

In this section we present the interpretable LVQ algorithm capable of dealing with missingness and proposed extensions for non-linear decision boundaries and visualisation. We assume training is based on S data samples $\{\mathbf{x}_i \in \mathbb{R}^D\}_{i=1}^S$ accompanied by a label $c(\mathbf{x}_i)$ belonging to one of C classes and a set of adaptive prototypes $\mathbf{w} \in \mathbb{R}^D$ with labels $c(\mathbf{w})$. A new data sample receives a label following a prototype-based nearest neighbor classification scheme: by assigning the label of the closest prototype with $c(\mathbf{w}_J) = \arg \min_J d_i^J$ using a dissimilarity measure $d_i^J = d(\mathbf{x}_i, \mathbf{w}_J)$. The paper by [8] introduced Generalized LVQ (GLVQ), in which the prototype positions were optimised using the following cost function:

$$E = \sum_{i=1}^S \Phi \left(\frac{d_i^J - d_i^K}{d_i^J + d_i^K} \right), \quad (1)$$

with d_i^J being the Euclidean distance of each training sample to the closest prototype of the same class $c(\mathbf{x}_i) = c(\mathbf{w}_J)$ and d_i^K the closest prototype with another class label. Φ is a monotonic function and we set it to the identity $\Phi(a) = a$ throughout this contribution. Learning takes place by adapting the prototypes \mathbf{w} , e.g. by stochastic gradient descent updating the closest correct and wrong prototypes \mathbf{w}^L , $L \in \{J, K\}$ using the derivatives $\nabla \mathbf{w}^L = \frac{\partial E}{\partial \mathbf{w}^L}$:

$$\begin{aligned} \frac{\partial E}{\partial \mathbf{w}^J} &= \sum_{i=1}^S \gamma_i^J \frac{\partial d_i^J}{\partial \mathbf{w}^J} \text{ and } \frac{\partial E}{\partial \mathbf{w}^K} = \sum_{i=1}^S \gamma_i^K \frac{\partial d_i^K}{\partial \mathbf{w}^K} \text{ with} \\ \gamma_i^J &= \frac{2d_i^K}{(d_i^J + d_i^K)^2} \text{ and } \gamma_i^K = \frac{-2d_i^J}{(d_i^J + d_i^K)^2} \end{aligned} \quad (2)$$

After training the prototypes can often be considered typical representatives of their class and their characteristics can be investigated for interpretation.

Since the Euclidean distance is sensitive to missing values the authors introduced an angle-based variant ALVQ allowing learning in variable dimensional spaces [12, 13]:

$$d_i^L = g_\beta(b) = \frac{e^{(-\beta(b-1))} - 1}{e^{(2\beta)} - 1} \text{ with } b = \frac{\mathbf{x}_i \cdot \mathbf{w}^L}{\|\mathbf{x}_i\| \|\mathbf{w}^L\|}. \quad (3)$$

The exponential function $g_\beta(b)$ transforms the angle $b = \cos \theta \in [-1, 1]$ into dissimilarities in $[0, 1]$ with the hyper-parameter β influencing the slope, e.g. $\beta \rightarrow 0$ leading to a near linear relationship. In presence of missing data the angle b and derivatives are computed with the available dimensions only. Optimization takes place deriving the cost function E Eq. (1-2) with changed

dissimilarity d_i^L adding:

$$\frac{\partial d_i^L}{\partial \mathbf{w}^L} = \frac{\partial g_\beta(b)}{\partial b} \cdot \frac{\partial b}{\partial \mathbf{w}^L} \text{ and} \quad (4)$$

$$\frac{\partial g_\beta(b)}{\partial b} = \frac{-\beta \exp(-\beta b + \beta)}{\exp(2\beta) - 1}. \quad (5)$$

The update rules of GLVQ contains forces attracting the closest correct prototype for each data sample and repulsion of the closest one with a different class label. For example in an imbalanced 2 class problem the Euclidean variant might push the minority class prototype far away from the data all together, since it is being repelled more often by the majority class than attracted by the minority class. ALVQ classifies on the hypersphere, so a prototype cannot be infinitely repelled without returning on the other side, leading to more stable behaviour facing imbalance. Finally, the dissimilarity measure d_i^L can be parameterized leading to several powerful extensions with varying potential for further interpretation. We group the novel angle extensions into three categories, namely global, local and 2 matrix, as explained in the following subsections.

2.1 Global relevance matrix

First extensions to GLVQ introduced parameterized dissimilarity measures based on the quadratic form:

$$d_i^L = (\mathbf{x}_i - \mathbf{w}^L)^\top \Lambda (\mathbf{x}_i - \mathbf{w}^L), \quad (6)$$

with the semi-definite matrix $\Lambda \in \mathbb{R}^{D \times D}$ containing additional parameters for optimization. A variant called Relevance GLVQ (GRLVQ) [9] assumes Λ to be a diagonal matrix with $\sum_{i=1}^D \Lambda_{ii}^2 = 1$. The diagonal elements $r_i = \Lambda_{ii}^2$ allow learning of discriminant feature directions, which automatically reduces the influence of less relevant measurement dimensions. However GRLVQ is univariate and does not take into account features which are relevant only in combination with another. Generalized Matrix LVQ (GMLVQ) [10, 11, 14] tackles this issue by allowing a full matrix Λ , ensuring semi-definiteness by the decomposition $\Lambda = \Omega^\top \Omega$ and optimizing E with respect to $\Omega \in \mathbb{R}^{D \times D}$. Since d_i^L can be rewritten as squared Euclidean distance in the space linearly transformed by Ω : $d_i^L = (\Omega \mathbf{x}_i - \Omega \mathbf{w}^L)^2$, [5] used the concept for discriminant visualisation. This is achieved by limiting the rank of Λ using a rectangular matrix $\Omega \in \mathbb{R}^{M \times D}$ with $M \leq D$, which in turn can be used to visualise the piecewise linear decision boundaries if $M \in \{2, 3\}$.

Similarly, to extend ALVQ to global relevances we proposed a parameterized computation of the angle [12, 13]:

$$b = b_\Omega = \frac{\mathbf{x}_i^\top \Omega^\top \Omega \mathbf{w}^L}{\|\mathbf{x}_i\|_\Omega \|\mathbf{w}^L\|_\Omega} \text{ with } \|\mathbf{v}\|_\Omega = \sqrt{\mathbf{v}^\top \Omega^\top \Omega \mathbf{v}}, \quad (7)$$

with corresponding derivatives:

$$\begin{aligned} \frac{\partial b_\Omega}{\partial \mathbf{w}^L} &= \frac{\mathbf{x}_i \Omega^\top \Omega \|\mathbf{w}^L\|_\Omega^2 - \mathbf{x}_i \Omega^\top \Omega \mathbf{w}^L \cdot \mathbf{w}^L \Omega^\top \Omega}{\|\mathbf{x}_i\|_\Omega \|\mathbf{w}^L\|_\Omega^3} \quad (8) \\ \frac{\partial b_\Omega}{\partial \Omega_{md}} &= \frac{x_{i,m} \sum_j \Omega_{jd} w_j^L + w_m^L \sum_j \Omega_{jd} x_{i,j}}{\|\mathbf{x}_i\|_\Omega \|\mathbf{w}^L\|_\Omega} - \mathbf{x}_i \Omega^\top \Omega \mathbf{w}^L \\ &\quad \cdot \left[\frac{x_{i,m} \sum_j \Omega_{jd} x_{i,j}}{\|\mathbf{x}_i\|_\Omega^3 \|\mathbf{w}^L\|_\Omega} + \frac{w_m^L \sum_j \Omega_{jd} w_j^L}{\|\mathbf{x}_i\|_\Omega \|\mathbf{w}^L\|_\Omega^3} \right], \quad (9) \end{aligned}$$

where $x_{i,m}$ denotes dimension m of vector \mathbf{x}_i . As before the diagonal of $\Lambda = \Omega^\top \Omega$ denotes the individual feature relevances

for the classification and Ω can be rectangular $\Omega \in \mathbb{R}^{M \times D}$ with $M \leq D$ to be used for visualisation. Resulting visualisations are one M dimensional hyper-spheres where the angle-based classification takes place. The global Euclidean and angle implementation will be abbreviated by LVQ_g and ALVQ_g respectively.

2.2 Local relevance matrix

The localized extension LGMLVQ [11] allows more complex modeling and prototype or class-wise feature relevance determination by attaching metric tensors Ψ^c to each prototype or each class (based on the user's choice):

$$d_i^c = (\mathbf{x}_i - \mathbf{w}^c)^\top \Psi^c \Psi^c (\mathbf{x}_i - \mathbf{w}^c) . \quad (10)$$

This Euclidean variant is powerful for finding solutions to non-linearly separable multi-class problems. The diagonal of the local metric tensors $\Lambda_c = \Psi^c \Psi^c$ contain local or class-wise feature relevances, which can be investigated by the user for class-specific discriminative information. However, visualising the decision boundaries is not trivial and non-linear mappings based on charting can be found in [5, 15].

In this contribution we extend ALVQ learning with missing data to local relevances following similar principles:

$$b = b_{\Psi^L} = \frac{\mathbf{x}_i^\top \Psi^L \Psi^L \mathbf{w}^L}{\|\mathbf{x}_i\|_{\Psi^L} \|\mathbf{w}^L\|_{\Psi^L}} . \quad (11)$$

The corresponding derivatives of b_{Ψ^L} are as follows:

$$\frac{\partial b_{\Psi^L}}{\partial \mathbf{w}^L} = \frac{\mathbf{x}_i \Psi^L \Psi^L \|\mathbf{w}^L\|_{\Psi^L}^2 - \mathbf{x}_i \Psi^L \Psi^L \mathbf{w}^L \cdot \mathbf{w}^L \Psi^L \Psi^L}{\|\mathbf{x}_i\|_{\Psi^L} \|\mathbf{w}^L\|_{\Psi^L}^3} \quad (12)$$

$$\frac{\partial b_{\Psi^L}}{\partial \Psi_{md}^L} = \frac{x_{i,m} \sum_j \Psi_{jd}^L w_j^L + w_m^L \sum_j \Psi_{jd}^L x_{i,j}}{\|\mathbf{x}_i\|_{\Psi^L} \|\mathbf{w}^L\|_{\Psi^L}} - \mathbf{x}_i \Psi^L \Psi^L \mathbf{w}^L \left[\frac{x_{i,m} \sum_j \Psi_{jd}^L x_{i,j}}{\|\mathbf{x}_i\|_{\Psi^L}^3 \|\mathbf{w}^L\|_{\Psi^L}} + \frac{w_m^L \sum_j \Psi_{jd}^L w_j^L}{\|\mathbf{x}_i\|_{\Psi^L} \|\mathbf{w}^L\|_{\Psi^L}^3} \right] \quad (13)$$

Similarly to the Euclidean version the local matrices can lead to valuable insight about local or class-wise relevant features and visualisation of the non-linear decision boundaries needs additional effort. The local Euclidean and angle implementation will be abbreviated by LVQ_l and ALVQ_l respectively.

2.3 2 matrix decomposition for visualisation

As a compromise between linear dimensionality reduction and visualisation of non-linear decision boundaries [5] introduced a composition of the matrix in the quadratic form Eq. (6) with two matrices:

$$d_i^c = (\mathbf{x}_i - \mathbf{w}^c)^\top \Omega^\top \Psi^c \Psi^c \Omega (\mathbf{x}_i - \mathbf{w}^c) , \quad (14)$$

with $\Omega \in \mathbb{R}^{M \times D}$ and $\Psi^c \in \mathbb{R}^{M \times M}$. The data and prototypes are therefore transformed linearly to the M -dimensional space and the local metric tensors define the non-linear decision boundaries in that space. If the intrinsic dimensionality is more than $M \in \{2, 3\}$ a loss of information in classification and visualisation is inevitable, however the cost function ensures that this loss is minimized.

In this contribution we similarly extend ALVQ for visualisation with non-linear decision boundaries:

$$b = b_{2M} = \frac{\mathbf{x}_i^\top \Omega^\top \Psi^L \Psi^L \Omega \mathbf{w}^L}{\|\mathbf{x}_i\|_{2M} \|\mathbf{w}^L\|_{2M}} \quad (15)$$

with $\|\mathbf{v}\|_{2M} = \sqrt{\mathbf{v}^\top \Omega^\top \Psi^L \Psi^L \Omega \mathbf{v}}$ and derivatives:

$$\frac{\partial b_{2M}}{\partial \mathbf{w}^L} = \frac{\mathbf{x}_i \Omega^\top \Psi^L \Psi^L \Omega \|\mathbf{w}^L\|_{2M}^2 - \mathbf{x}_i \Omega^\top \Psi^L \Psi^L \Omega \mathbf{w}^L \cdot \mathbf{w}^L \Omega^\top \Psi^L \Psi^L \Omega}{\|\mathbf{x}_i\|_{2M} \|\mathbf{w}^L\|_{2M}^3} \quad (16)$$

$$\frac{\partial b_{2M}}{\partial \Omega} = \frac{2\mathbf{x}_i^\top \Psi^L \Psi^L \Omega \mathbf{w}^L}{\|\mathbf{x}_i\|_{2M} \|\mathbf{w}^L\|_{2M}} - \mathbf{x}_i \Omega^\top \Psi^L \Psi^L \Omega \mathbf{w}^L \cdot \left[\frac{\mathbf{x}_i \Psi^L \Psi^L \Omega \mathbf{x}_i}{\|\mathbf{x}_i\|_{2M}^3 \|\mathbf{w}^L\|_{2M}} + \frac{\mathbf{w}^L \Psi^L \Psi^L \Omega \mathbf{w}^L}{\|\mathbf{x}_i\|_{2M} \|\mathbf{w}^L\|_{2M}^3} \right] \quad (17)$$

$$\frac{\partial b_{2M}}{\partial \Psi^L} = \frac{2\mathbf{x}_i^\top \Omega^\top \Psi^L \Omega \mathbf{w}^L}{\|\mathbf{x}_i\|_{2M} \|\mathbf{w}^L\|_{2M}} - \mathbf{x}_i \Omega^\top \Psi^L \Psi^L \Omega \mathbf{w}^L \cdot \left[\frac{\mathbf{x}_i \Omega^\top \Psi^L \Omega \mathbf{x}_i}{\|\mathbf{x}_i\|_{2M}^3 \|\mathbf{w}^L\|_{2M}} + \frac{\mathbf{w}^L \Omega^\top \Psi^L \Omega \mathbf{w}^L}{\|\mathbf{x}_i\|_{2M} \|\mathbf{w}^L\|_{2M}^3} \right] \quad (18)$$

The 2 matrix Euclidean and angle implementation will be abbreviated by LVQ_{2M} and ALVQ_{2M} respectively.

3 Datasets

We demonstrate our newly developed classifiers on two datasets: a synthetic 2-class dataset and a publicly available multi-class heart disease dataset as explained in the following subsections.

3.1 Synthetic non-linear dataset (Football)

We used the open-source software system Chebfun [16] to create a synthetic 2 class dataset resembling the pattern of a football (see Fig.1). The function producing the pattern is $f(\mathbf{x}) = 2 \sinh(5x_1 \cdot x_2 \cdot x_3)$ with $f(\mathbf{x}) \leq 0.5$ belonging to class 0 and $f(\mathbf{x}) > 0.5$ to class 1. We created 5000 samples for train-

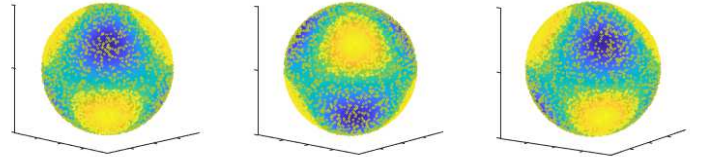


Fig. 1: Football: 3 different views of a non-linearly separable synthetic dataset.

ing and validation splits in cross-validation and additional 25000 samples serve as hold-out test set to investigate the generalization ability of the classifier. The data is available online*. Performance on this dataset is reported in terms of training and test errors, as well as sensitivity and specificity.

3.2 Heart disease dataset from UCI

This dataset, also known as the Cleveland heart disease (HD) dataset [17], contains 303 subjects in total (164 healthy, and 139 with varying degrees of heart problems). The predictor variable is originally 5 unique values, 0 indicating healthy (164), while 1 (55 subjects), 2 (36 subjects), 3 (35 subjects), and 4 (13 subjects) indicating patients with different heart conditions. Furthermore, six subjects contain missing values. The dataset originally consists of 76 features but most research has been done on a subset of 13 of these. For easy comparison we investigate the same 13 features and details about them can be found at the UCI repository [17].

* github.com/sreejita-rug/Synthetic-Chebfun-football.git

Exploratory analysis showed that while there is a very good separation between healthy and HD subjects considered in binary classification, the multi-class problem differentiating between the 4 classes of HD patients turns out to be remarkably difficult. Therefore, besides the more interesting multi-class problem, we added an investigation of the binary sub-problem to compare the performance to the majority of earlier results reported on this dataset. However, unlike most contributions we did not discard entries with missing values, since our method can be trained in variable dimensional spaces. According to [17] the missing values in the data were replaced by a value of -9. For the binary problem we report the performance keeping this, to compare to earlier results. In the multi-class analysis however we revert the -9s to NaNs.

Literature on the heart disease dataset investigating the binary problem, showed good performance by SVMs with non-linear kernels, neural networks, k-nearest neighbour (kNN) using $k = 16, 19, 28$, Fischer Discriminant Analysis (FDA), Linear Discriminant Analysis (LDA), NB and ensemble classifiers such as RF [18–20]. Although these classifiers perform well in binary classification of this HD dataset, direct interpretation and visualization of the trained models remains difficult, with exception of the RF. Models with enhanced interpretability as proposed in this contribution can alternatively deliver additional insight. This is also demonstrated on the more interesting multi-class problem.

4 Experiments

In this section we explain the experimental setup for the synthetic and heart disease dataset and the performance metrics used for comparison. Results are summarized in tables with abbreviations as introduced before: global feature relevances Euclidean and angle based (LVQ_g and ALVQ_g), local relevances (LVQ_l and ALVQ_l), Random Forest (RF), and the 2 matrix versions providing visualisations of the nonlinear decision boundaries (LVQ_{2M} and ALVQ_{2M}). The superscripts denote the value of hyperparameters β for ALVQ and the number of trees in the RF classifier.

4.1 Synthethic data

We demonstrate the difference of the localized and 2 matrix Euclidean LVQ versions and our angle based extensions on the synthetic football pattern data set. Therefore, we performed a 10-fold cross validation for comparison and model selection with 5000 samples. The generalization ability of the selected model is evaluated on 25000 hold-out test samples and performance is reported in terms of training and test errors, as well as sensitivity and specificity. We use 3 prototypes per class ($\varphi = 6$) and class-wise matrices on this dataset.

4.2 Heart disease data

We compare the proposed angle LVQ variants with results from the literature [20, 21]. Contrary to past results our method can perform on the existing dimensions only. This avoids imputation and offers additional insights in the form of feature relevance determination and visualisation of the decision boundaries. This dataset was z-score transformed in each fold using the mean and standard deviation of the corresponding training set. Earlier results were typically acquired by 10-fold cross validation, since most of them simplify the problem to two classes, combining all diseases into one. However, we use 5-fold cross validation, since

Table 1: Experiments performed on the heart disease dataset.

classes	Method	Hyperparameters	Preprocessing
Binary	LVQ _g	φ , rank of Ω	z-score
Binary	ALVQ _g	φ , rank of Ω , β	z-score
Binary	RF	No. of trees	z-score
5-class	ALVQ _g	φ , rank of Ω , β	z-score, SMOTE ^g
5-class	ALVQ _l	φ , ranks of $\{\Psi_c\}$, β	z-score, SMOTE ^g
5-class	ALVQ _{2M}	φ , ranks of $\Omega \& \{\Psi_c\}$, φ , β	z-score, SMOTE ^g
5-class	RF	No. of trees	z-score, SMOTE ^s

the smallest minority class contained only 14 subjects justifying only a lower number of folds for the analysis of the multi-class problem. Albeit the multi-class problem being severely more difficult we show that the enhanced interpretability offers additional insight into the problem.

Table 1 shows an overview of the experiments performed and intrinsic method hyperparameters. The imbalance of the classes is handled by the Synthetic Minority Oversampling TEchnique (SMOTE) as described in [22]. SMOTE^g denotes a geodesic variant for oversampling on a hypersphere as introduced and explained in [12]. They were used to oversample all minority classes in the training set to contain the same number of samples as the majority class (Healthy). Based on exploratory analysis we chose $k = 3$ nearest neighbours for both SMOTE and SMOTE^g. We investigated the intrinsic dimensionality by training full rank matrices Ω for which subsequent Eigen-value decomposition of the resulting metric tensor Λ delivered insight into the required dimensions for classification. Afterwards we limit the rank for visualisation purpose. We experimented with varying number of prototypes per class (1, 2 and 3), such that $\varphi \in \{2, 4, 6\}$ for the binary class problem, and $\varphi \in \{5, 10, 15\}$ for 5-class problem, and investigated the influence of the hyperparameter β with $\beta \in \{1, 5, 10, 50, 80, 100\}$. As proposed in [23] we set minimum observation(s) per tree leaf in RF to 1, and number of random variables at each decision split to $\sqrt{D} = \sqrt{13} \approx 4$.

5 Results and Discussion

This section contains the detailed comparison of results from experiments performed on both datasets, followed by discussion and visualizations as enabled by the proposed ALVQ_{2M}. For the real-world heart disease we also showed a detailed investigation of interpretable parameters leading to further insight into the classification performed. RFs, which are also interpretable to some extent, makes it possible to extract feature importance. Therefore we were able to compare findings from the ALVQs and RFs.

5.1 Synthetic football dataset results

Table 2 summarizes the performance of the classifiers in terms of error on training and test set during cross validation and report the sensitivity and specificity with respect to the hold-out test set. We included the results using different hyperparameters β to provide information about the robustness and selected the model exhibiting best training performance as highlighted in boldface. As expected, earlier LVQ extensions perform worse on this non-Euclidean data set as depicted in the first 2 rows. The local relevance angle LVQ (ALVQ_l) clearly outperforms the other two being the most complex and flexible model with the largest number of parameters handling the nonlinearities of this data best. However, as mentioned before, visualization of the deci-

Table 2: Football comparison: mean performance (standard deviation)

Method	E_{train}	E_{test}	Sensitivity	Specificity
LVQ_{2M}	0.272 (0.019)	0.277 (0.027)	0.68 (0.093)	0.76 (0.103)
LVQ_l	0.223 (0.047)	0.224 (0.050)	0.78 (0.118)	0.76 (0.113)
$ALVQ_{10}^g$	0.268 (0.035)	0.273 (0.036)	0.78 (0.115)	0.67 (0.103)
$ALVQ_{30}^g$	0.273 (0.040)	0.285 (0.047)	0.76 (0.127)	0.68 (0.115)
$ALVQ_{50}^g$	0.271 (0.040)	0.279 (0.041)	0.76 (0.118)	0.69 (0.111)
$ALVQ_{80}^g$	0.284 (0.048)	0.290 (0.051)	0.74 (0.139)	0.68 (0.145)
$ALVQ_{100}^g$	0.277 (0.042)	0.288 (0.046)	0.75 (0.130)	0.68 (0.135)
$ALVQ_{120}^g$	0.286 (0.047)	0.298 (0.048)	0.74 (0.123)	0.66 (0.123)
$ALVQ_{10}^l$	0.199 (0.056)	0.202 (0.060)	0.82 (0.117)	0.77 (0.111)
$ALVQ_{30}^l$	0.176 (0.066)	0.182 (0.070)	0.82 (0.140)	0.82 (0.113)
$ALVQ_{50}^l$	0.197 (0.059)	0.204 (0.064)	0.79 (0.144)	0.80 (0.117)
$ALVQ_{80}^l$	0.196 (0.062)	0.208 (0.064)	0.79 (0.129)	0.80 (0.108)
$ALVQ_{100}^l$	0.191 (0.059)	0.200 (0.060)	0.79 (0.141)	0.82 (0.100)
$ALVQ_{120}^l$	0.201 (0.057)	0.208 (0.061)	0.77 (0.142)	0.81 (0.110)
$ALVQ_{30}^{2M}$	0.24 (0.057)	0.24 (0.059)	0.80 (0.124)	0.72 (0.116)
$ALVQ_{50}^{2M}$	0.23 (0.052)	0.23 (0.056)	0.77 (0.140)	0.76 (0.122)
$ALVQ_{80}^{2M}$	0.22 (0.058)	0.22 (0.061)	0.79 (0.133)	0.75 (0.117)
$ALVQ_{100}^{2M}$	0.24 (0.058)	0.25 (0.062)	0.76 (0.146)	0.74 (0.136)
$ALVQ_{120}^{2M}$	0.24 (0.058)	0.24 (0.060)	0.78 (0.140)	0.73 (0.130)
$ALVQ_{50}^{2M}$	0.24 (0.061)	0.24 (0.063)	0.77 (0.141)	0.73 (0.140)

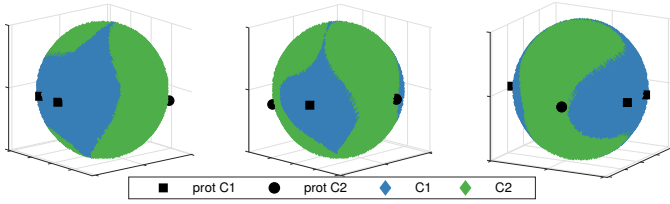


Fig. 2: Three different perspectives of the nonlinear decision boundaries in the spherical classification space of $ALVQ_{2M}$ trained on the Football dataset.

sion boundaries with local metric tensors is not straightforward. Therefore we demonstrate the 2 matrix extension $ALVQ_{2M}$ with complexity and performance in between the global and local variants. Figure 2 shows a corresponding example visualization of the nonlinear decision boundaries and prototypes in the spherical classification space seen from 3 different perspectives. Individual data samples have been omitted in the illustration to reduce visual clutter, but can be added of course for investigation.

5.2 Heart disease (binary class problem) results

First, we investigated the binary subproblem combining all diseases to one class and estimate the intrinsic dimensionality by investigating the eigenvalue profile of the trained $\Lambda = \Omega^T \Omega$ with full rank $\Omega \in \mathbb{R}^{D \times D}$ and one prototype per class. Since there is not enough data to create a hold-out generalization set we report the sensitivity and specificity of the classifiers as observed on the test set of the cross-validation splits. Figure 3 shows box plots of the estimates of the intrinsic dimensionality according to different settings of the hyperparameter β and the average performance of corresponding models is summarized in Table 3.

Even though there are 13 features in the dataset much lower dimensionality seems necessary for classification as indicated by most Eigenvalues being close to 0. The best performing β depicts only three Eigenvalues significantly bigger than 0 indicating the problem can be visualized in three dimensions with limited loss of information. Thus we re-train the models by limiting the rank to three ($M = 3$).

As before we perform model selection and highlight in boldface based on the best training set performance and report sensitiv-

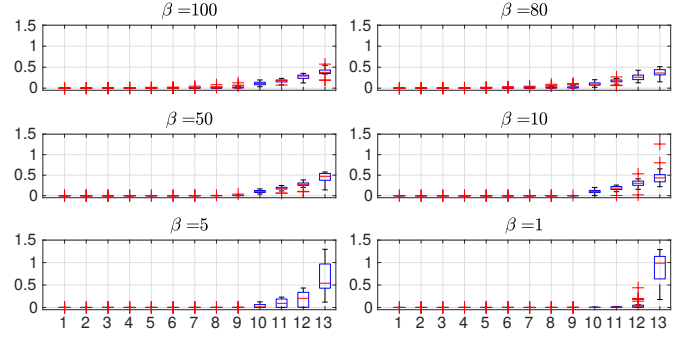


Fig. 3: Eigenvalues of Λ across 5 folds and 5 runs.

Table 3: binary HD: mean performance (std) of global full rank $ALVQ$

Method	E_{train}	E_{test}	Sensitivity	Specificity
$ALVQ_g$	0.112 (0.009)	0.171 (0.029)	0.79 (0.084)	0.86 (0.094)
$ALVQ_g^5$	0.110 (0.010)	0.178 (0.044)	0.78 (0.097)	0.86 (0.086)
$ALVQ_{10}^g$	0.112 (0.015)	0.188 (0.040)	0.78 (0.120)	0.84 (0.098)
$ALVQ_{30}^g$	0.130 (0.018)	0.181 (0.044)	0.80 (0.066)	0.83 (0.089)
$ALVQ_{50}^g$	0.133 (0.019)	0.180 (0.046)	0.80 (0.076)	0.84 (0.090)
$ALVQ_{100}^g$	0.140 (0.025)	0.202 (0.050)	0.77 (0.088)	0.82 (0.081)

Table 4: binary HD: mean performance (std) final comparison

Method	E_{train}	E_{test}	Sensitivity	Specificity
LVQ_g	0.459 (0.001)	0.459 (0.005)	0.00 (0.000)	1.00 (0.000)
$ALVQ_g^5$	0.114 (0.009)	0.169 (0.034)	0.81 (0.077)	0.85 (0.098)
$ALVQ_{10}^g$	0.116 (0.012)	0.178 (0.048)	0.79 (0.110)	0.85 (0.088)
$ALVQ_{30}^g$	0.122 (0.013)	0.187 (0.050)	0.79 (0.101)	0.83 (0.095)
$ALVQ_{50}^g$	0.145 (0.023)	0.199 (0.044)	0.80 (0.081)	0.80 (0.074)
$ALVQ_{80}^g$	0.168 (0.029)	0.210 (0.052)	0.76 (0.096)	0.81 (0.080)
$ALVQ_{100}^g$	0.163 (0.033)	0.204 (0.052)	0.79 (0.075)	0.80 (0.066)
RF_{50}^l	0.001 (0.002)	0.179 (0.044)	0.78 (0.084)	0.86 (0.058)
RF_{100}^l	0.0 (0.0)	0.179 (0.044)	0.77 (0.082)	0.86 (0.048)
RF_{150}^l	0.0 (0.0)	0.170 (0.043)	0.78 (0.081)	0.87 (0.046)
RF_{200}^l	0.0 (0.0)	0.177 (0.050)	0.77 (0.082)	0.86 (0.053)
NB^{Kol}	NA	NA	0.86	0.833
MLP^{Kol}	NA	NA	0.836	0.80

ity and specificity on the respective test splits. Reducing the rank of the matrix regularizes the model leading to improved generalization performance as depicted in Table 4. We also notice that the Euclidean versions of LVQ , i.e. $GMLVQ$, exhibits poor performance on this data set. This might be due to the presence of missing data, which the angle version is able to deal with. RF with 100 and more trees have had perfect training, but the sensitivity on the validation set is similar to that of angle LVQ . We also observe similar performance in comparison with results reported in [19] for the NB and Multi Layer Perceptron (MLP) marked as NB^{Kol} and MLP^{Kol} . They used 10-fold cross-validation, but standard deviation across the different splits or training and test error were not reported.

Classifiers of the LVQ family can also identify relevant features for a particular task, along with finding typical representatives of each class (prototypes). Figure 4 shows the feature relevances and prototypes of the healthy and disease class learned during training corresponding to the best setting ($ALVQ_g^5$) in Table 4.

The features 3 (Chest pain type), 12 (number of major vessels as coloured by fluoroscopy) and 13 (status of heart, w.r.t the

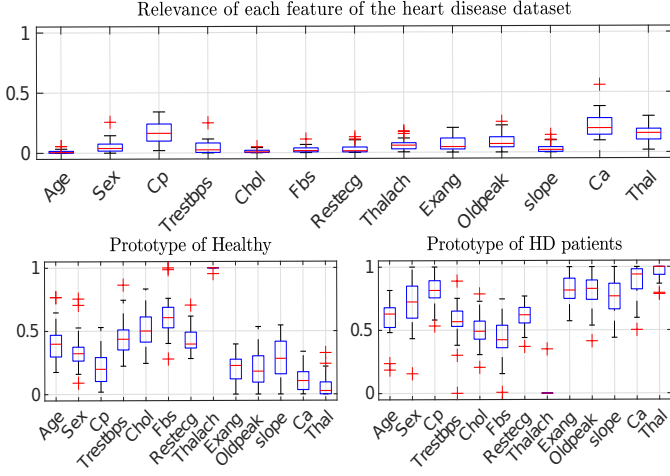


Fig. 4: Feature relevances (top panel), as well as healthy and disease prototypes (bottom row) obtained by $ALVQ_g^1$ on the binary HD classification.

organ being normal having had the anomaly fixed, and having a reversible defect) are among the most highly relevant ones, followed by features 2 (sex), 8 (maximum heart rate achieved) and 9 (exercise induced angina). Important features extracted from RF models are shown in Fig. 5. RF and ALVQ feature sets agree with regard to features 3, 8, 9, 10, 12, and 13 being the more distinguishing ones, whereas features 4, 5 and 7 do not contribute as much. In contrast to RF we can also investigate the prototypes of the healthy and patient class. Notably, the features found also visibly differ in the adapted prototypes of the healthy and patient. We see in Figure 4, that feature 3 value lie below the 0.5 mark for class-Healthy whereas it is higher than 0.5 mark for the HD prototype. Similarly for value of features 12, 13, 2, and 9. For features 8 and 10 the opposite trend is seen: the maximum heart rate achieved for the prototype describing the healthy subjects was much higher than the 0.5 mark whereas for the patients it was significantly lower than that mark. Conversely, features which were not deemed highly relevant by our classifier, such as features 1 (age), 4 (resting blood pressure), and 7 (resting ECG), are seen to have values in the mid-part of the prototype plots for both the classes, thus indicating that they are not as integral to distinguishing between healthy subjects and HD patients. These findings also agree with those mentioned in [20, 21].

5.3 Heart disease (5-class problem) results

More challenging and potentially more interesting is the investigation of the 5 class problem keeping the original HD sub-classes. Since there are 5 classes we show the performance in terms of training and test errors, and class-wise accuracies. The class-wise accuracy of the Healthy class (C0) is the same as specificity and therefore omitted in the following. Table 5 shows that the class-wise accuracies during validation are better from the more complex local model of angle LVQ ($ALVQ_l$), whose prototypes and local relevances are depicted in Figure 7. Additional interpretation can be gained by using the proposed 2 matrix variant $ALVQ_{2M}$. For this problem we compared using 1, 2 and 3 prototypes per class, since it depicted the best averaged class-wise accuracy on training. The study in [20] attempts to investigate the disease classes considering one class versus all classification. Their highest sensitivity per condition in this simplified setting were reported to be: 0.891 (Healthy, Sequential minimal optimization (SMO)), 0.321 (HD class 1, IBK from Weka), 0.405 (HD class 2, NB), 0.472 (HD class 3, NB) and 0.214 (HD class 4, IBK) furthermore confirming the complexity of the multi-class problem we investigate. Table 5 shows that the performance of RF and the ALVQ classifiers were comparable in sensitivity and specificity in the more complex 5-class setting. However the ALVQ models can provide additional insight by prototypes and visualizations.

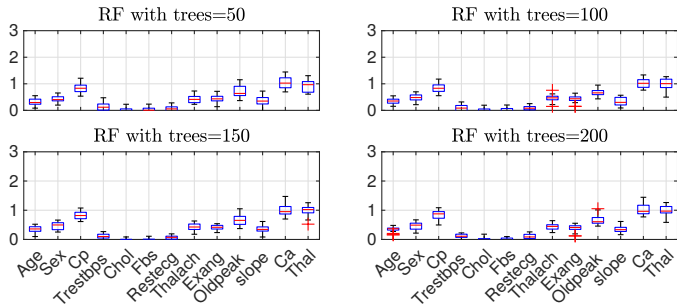
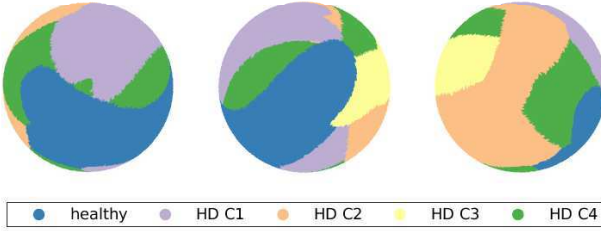
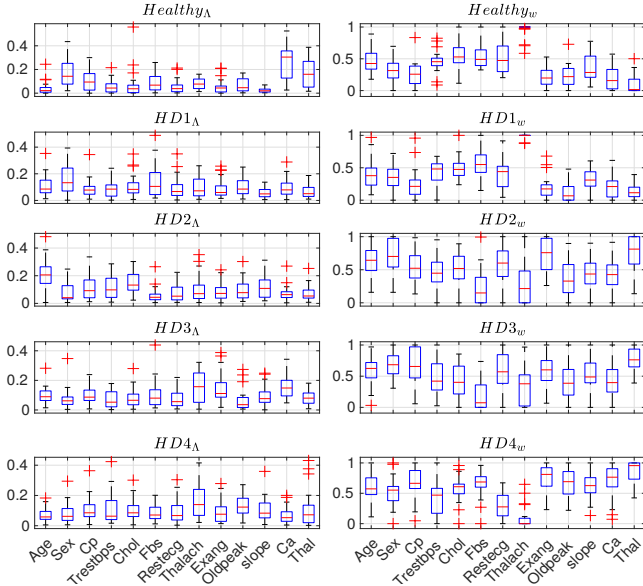
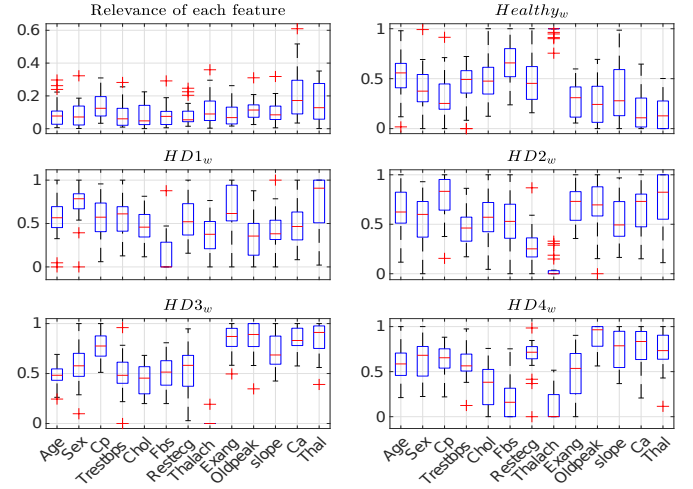


Fig. 5: Summary of the feature importance determined by RF over 5 folds and 5 runs, trained for the binary class problem.

Figure 6 shows the decision boundaries of an example $ALVQ_{2M}$ using $\beta = 5$ showing best performance according to Table 5. The picture confirms the non-linearity of this dataset when investigated as 5-class problem. Individual data samples are again omitted to avoid visual clutter but can be added and investigated with respect to their distance to the decision boundaries. The corresponding cross-validation relevances of $\Omega^T \Omega$ and prototypes are depicted in Figure 8. Next we investigate the models trained for the multi-class problem in more detail to hypothesize why this problem is so difficult. Figure 7 illustrates

Table 5: 5-class HD: mean performance (std) comparison of ALVQ variants and RF

Method	E_{train}	E_{test}	Sens	Spec	C1	C2	C3	C4
$ALVQ_{l^{100}}^g$	0.34 (0.032)	0.54 (0.081)	0.07 (0.043)	0.68 (0.130)	0.19 (0.111)	0.22 (0.209)	0.20 (0.180)	0.25 (0.260)
$ALVQ_{l^{80}}^g$	0.33 (0.034)	0.52 (0.075)	0.08 (0.048)	0.69 (0.090)	0.21 (0.125)	0.23 (0.167)	0.26 (0.188)	0.29 (0.298)
$ALVQ_{l^{150}}^g$	0.32 (0.043)	0.53 (0.061)	0.08 (0.053)	0.71 (0.090)	0.20 (0.134)	0.18 (0.148)	0.22 (0.143)	0.13 (0.204)
$ALVQ_{l^{10}}^g$	0.35 (0.071)	0.48 (0.056)	0.08 (0.060)	0.76 (0.063)	0.21 (0.154)	0.21 (0.168)	0.26 (0.196)	0.23 (0.281)
$ALVQ_{l^5}^g$	0.35 (0.071)	0.50 (0.074)	0.04 (0.045)	0.77 (0.097)	0.11 (0.112)	0.19 (0.153)	0.26 (0.210)	0.29 (0.313)
$ALVQ_{l^1}^g$	0.37 (0.063)	0.49 (0.053)	0.05 (0.049)	0.79 (0.088)	0.12 (0.125)	0.19 (0.167)	0.25 (0.161)	0.22 (0.288)
$ALVQ_{l^{100}}^l$	0.24 (0.048)	0.51 (0.067)	0.08 (0.060)	0.69 (0.090)	0.20 (0.155)	0.31 (0.131)	0.34 (0.193)	0.13 (0.226)
$ALVQ_{l^{80}}^l$	0.21 (0.034)	0.49 (0.049)	0.09 (0.071)	0.73 (0.066)	0.22 (0.186)	0.31 (0.134)	0.28 (0.208)	0.15 (0.240)
$ALVQ_{l^{50}}^l$	0.18 (0.038)	0.49 (0.062)	0.09 (0.066)	0.72 (0.061)	0.22 (0.168)	0.26 (0.152)	0.33 (0.164)	0.17 (0.276)
$ALVQ_{l^{10}}^l$	0.16 (0.025)	0.48 (0.049)	0.08 (0.065)	0.76 (0.065)	0.20 (0.168)	0.28 (0.173)	0.31 (0.149)	0.05 (0.150)
$ALVQ_{l^5}^l$	0.16 (0.025)	0.49 (0.052)	0.07 (0.061)	0.74 (0.084)	0.17 (0.159)	0.30 (0.206)	0.34 (0.179)	0.05 (0.132)
$ALVQ_{l^1}^l$	0.17 (0.022)	0.50 (0.056)	0.07 (0.053)	0.74 (0.089)	0.18 (0.138)	0.23 (0.155)	0.31 (0.189)	0.08 (0.167)
$ALVQ_{2M}^{100}$	0.38 (0.064)	0.53 (0.071)	0.09 (0.066)	0.68 (0.109)	0.23 (0.172)	0.22 (0.190)	0.22 (0.160)	0.27 (0.315)
$ALVQ_{2M}^{80}$	0.36 (0.058)	0.55 (0.074)	0.06 (0.053)	0.67 (0.121)	0.15 (0.136)	0.21 (0.149)	0.25 (0.212)	0.23 (0.308)
$ALVQ_{2M}^{50}$	0.35 (0.059)	0.51 (0.075)	0.07 (0.063)	0.70 (0.122)	0.18 (0.161)	0.21 (0.154)	0.35 (0.207)	0.21 (0.232)
$ALVQ_{2M}^{10}$	0.34 (0.050)	0.51 (0.063)	0.07 (0.046)	0.72 (0.098)	0.17 (0.117)	0.24 (0.177)	0.26 (0.160)	0.24 (0.268)
$ALVQ_{2M}^5$	0.31 (0.033)	0.49 (0.073)	0.06 (0.052)	0.76 (0.108)	0.16 (0.133)	0.26 (0.168)	0.31 (0.198)	0.17 (0.252)
$ALVQ_{2M}^1$	0.32 (0.043)	0.49 (0.072)	0.06 (0.050)	0.75 (0.089)	0.15 (0.129)	0.26 (0.180)	0.30 (0.216)	0.30 (0.337)
RF^{50}	0.0 (0.002)	0.46 (0.039)	0.06 (0.044)	0.85 (0.054)	0.15 (0.112)	0.31 (0.110)	0.15 (0.095)	0.06 (0.134)
RF^{100}	0.0 (0.0)	0.46 (0.030)	0.03 (0.028)	0.88 (0.060)	0.07 (0.069)	0.30 (0.164)	0.09 (0.071)	0.0 (0.0)
RF^{150}	0.0 (0.0)	0.44 (0.022)	0.05 (0.036)	0.88 (0.049)	0.13 (0.095)	0.28 (0.120)	0.23 (0.117)	0.0 (0.0)
RF^{200}	0.0 (0.0)	0.45 (0.020)	0.04 (0.039)	0.87 (0.049)	0.09 (0.102)	0.33 (0.144)	0.20 (0.117)	0.10 (0.204)

Fig. 6: Three example perspectives of the classification sphere depicting the decision boundaries as determined by $ALVQ_{2M}$ on the 5-class HD problem.Fig. 7: Local relevances (left) and prototypes (right) of Healthy, and HD-patients of types 1-4, from $ALVQ_l$ over 5 folds, for the 5-class problem.Fig. 8: Global relevance, and prototypes (w) of Healthy and the 4 types of HD patients, from $ALVQ_{2M}^5$, over 5 folds, trained for the 5-class problem.

$ALVQ_l$ classifier with $\beta = 5$ and Ψ_c of dimension 3×13 , the hyperparameter setting which showed best performance among angle local LVQ according to Table 5. We compare the feature relevance from Ψ_c (Fig. 7) with those from figures 4 and 5. Features 3, 12, and 13 were among the most relevant features for the binary class problem. However, for the multi-class problem, on checking the prototype of each class, we see that these features do not have a distinct value boundary which could help in identification of the different classes. If we consider feature 12 (Ca) for all the prototypes we can see how easily healthy subjects and patients from class sick-1 would be confused, similarly patients of sick class 2 would be easily confused with those from sick class 3. According to Fig. 8 features 12 (Ca) and 13 (Thal) are still the most relevant ones. However the prototypes show that these features are good for distinguishing between healthy

and the rest of the classes, but not that efficient for differentiating between the heart disease classes themselves. These plots further explain why the specificity (or the class-wise accuracy of Healthy class) remained high even for the multi-class problem, whereas the class-wise accuracies were comparably poor for the remaining.

6 Conclusion and future Work

In this contribution we proposed three interpretable extensions of the angular nearest prototype based classifier, namely global angle LVQ, local angle LVQ and a 2 matrix version allowing visualisation of the non-linear decision boundaries. These set of classifiers are able to handle missingness as well as make knowledge extraction straightforward. As increasing number of human-centric sectors are becoming dependent on machine learning, understanding the exact working and underlying mechanisms behind a decision made by a model, are becoming paramount. Some classifiers depict comparable (and some even slightly higher) performance than these newly introduced classifiers. However, the proposed classifiers captivate due to their interpretability and the possibility to shed light on what exactly makes a classification problem difficult. This is highlighted in the given analysis of the 5 class heart disease identification problem where we achieve comparable performance to the RF. Even though the 13 out of 76 features were capable of distinguishing between healthy and heart disease patients, but features which can differentiate between all these 5 classes satisfactory seem not to be among these 14 features. Future contributions should investigate the larger feature set and the insight we can gain from it using interpretable classifiers.

Acknowledgment

We thank the Center for Information Technology of the University of Groningen for their support and for providing access to the Peregrine high performance computing cluster. We also thank the Rosalind Franklin fellowship, co-funded by the European Union's Seventh Framework Program for research, technological development and demonstration under grant agreement no **600211**, and H2020-MSCA-IF-2014, project ID **659104**.

References

- [1] Finale Doshi-Velez and Been Kim. Towards a rigorous science of interpretable machine learning. *arXiv preprint arXiv:1702.08608*, 2017.
- [2] Adrien Bibal and Benoît Frénay. Interpretability of machine learning models and representations: an introduction. In *ESANN*, 2016.
- [3] Diogo V Carvalho, Eduardo M Pereira, and Jaime S Cardoso. Machine learning interpretability: A survey on methods and metrics. *Electronics*, 8(8):832, 2019.
- [4] Andreas Backhaus and Udo Seiffert. Classification in high-dimensional spectral data: Accuracy vs. interpretability vs. model size. *Neurocomputing*, 131:15–22, 2014.
- [5] K. Bunte, P. Schneider, B. Hammer, F.-M. Schleif, T. Villmann, and M. Biehl. Limited Rank Matrix Learning, Discriminative Dimension Reduction and Visualization. *Neural Networks*, 26(4):159–173, February 2012.
- [6] Alexander Schulz, Andrej Gisbrecht, and Barbara Hammer. Using discriminative dimensionality reduction to visualize classifiers. *Neural Processing Letters*, 42(1):27–54, 2015.
- [7] Clément Bénard, Gérard Biau, Sébastien Da Veiga, and Erwan Scornet. Sirius: making random forests interpretable. *arXiv preprint arXiv:1908.06852*, 2019.
- [8] A. S. Sato and K. Yamada. Generalized learning vector quantization. In *Advances in Neural Information Processing Systems*, volume 8, pages 423–429, 1996.
- [9] B. Hammer and T. Villmann. Generalized relevance learning vector quantization. *Neural Networks*, 15(8–9):1059 – 1068, 2002.
- [10] P. Schneider, M. Biehl, and B. Hammer. Relevance matrices in learning vector quantization. In M. Verleysen, editor, *Proc. of the 15th European Symposium on Artificial Neural Networks (ESANN)*, pages 37–43, Bruges, Belgium, 2007. d-side publishing.
- [11] Petra Schneider, Michael Biehl, and Barbara Hammer. Adaptive relevance matrices in learning vector quantization. *Neural computation*, 21(12):3532–3561, 2009.
- [12] S. Ghosh, E.S. Baranowski, R. van Veen, Gert-Jan de Vries, M. Biehl, W. Arlt, P. Tino, and K. Bunte. Comparison of strategies to learn from imbalanced classes for computer aided diagnosis of inborn steroidogenic disorders. In Michel Verleysen, editor, *25th European Symposium on Artificial Neural Networks, Computational Intelligence and Machine Learning, ESANN 2017*, pages 199–205. Ciaco - i6doc.com, 4 2017.
- [13] K. Bunte, E. S. Baranowski, W. Arlt, and P. Tino. Relevance learning vector quantization in variable dimensional spaces. In Barbara Hammer, Thomas Martinetz, and Thomas Villmann, editors, *nc2, Workshop of the GI-Fachgruppe Neuronale Netze and the German Neural Networks Society in connection to GCPR 2016*, pages 20–23, Hannover, Germany, August 2016.
- [14] Petra Schneider, Michael Biehl, and Barbara Hammer. Distance learning in discriminative vector quantization. *Neural computation*, 21(10):2942–2969, 2009.
- [15] Kerstin Bunte, Barbara Hammer, Axel Wismüller, and Michael Biehl. Adaptive local dissimilarity measures for discriminative dimension reduction of labeled data. *Neurocomputing*, 73(7–9):1074–1092, 2010.
- [16] T. A. Driscoll, N. Hale, and L. N. Trefethen. *Chebfun guide*, 2014.
- [17] Andras Janosi, William Steinbrunn, Matthias Pfisterer, and Robert Detrano. Heart disease data set, UCI machine learning repository, 1988.
- [18] Mai Shouman, Tim Turner, and Rob Stocker. Applying k-nearest neighbour in diagnosing heart disease patients. *International Journal of Information and Education Technology*, 2(3):220–223, 2012.
- [19] Humar Kahramanli and Novruz Allahverdi. Design of a hybrid system for the diabetes and heart diseases. *Expert systems with applications*, 35(1-2):82–89, 2008.
- [20] Jesmin Nahar, Tasadduq Imam, Kevin S Tickle, and Yi-Ping Phoebe Chen. Computational intelligence for heart disease diagnosis: A medical knowledge driven approach. *Expert Systems with Applications*, 40(1):96–104, 2013.
- [21] Sellappan Palaniappan and Rafiah Awang. Intelligent heart disease prediction system using data mining techniques. In *2008 IEEE/ACS international conference on computer systems and applications*, pages 108–115. IEEE, 2008.
- [22] Nitesh V. Chawla, Kevin W. Bowyer, Lawrence O. Hall, and W. Philip Kegelmeyer. Smote: synthetic minority over-sampling technique. *Journal of artificial intelligence research*, 16:321–357, 2002.
- [23] Leo Breiman. Random forests. *Machine learning*, 45(1):5–32, 2001.